



UNIVERSITY OF GENOA

INGEGNERIA MECCANICA - ENERGIA E AERONAUTICA

60369-1718

FLUIDODINAMICA AVANZATA

---

**Constrained optimization of a 3D wing with winglet**

---

*Author:*  
Stefano Piccini

*Professor:*  
Jan Oscar Pralits

September 19, 2018

## Contents

<b>1</b>	<b>Physics behind</b>	<b>3</b>
1.1	Lift and Drag . . . . .	3
1.1.1	Lift and Drag Coefficients . . . . .	3
1.2	Induced Drag . . . . .	4
1.3	Winglets . . . . .	5
<b>2</b>	<b>Simulation set up</b>	<b>6</b>
2.1	Geometry . . . . .	6
2.2	OpenFOAM set up . . . . .	6
2.2.1	Unstructured Mesh . . . . .	8
2.2.2	SimpleFOAM set up . . . . .	9
2.3	Dakota optimization process . . . . .	10
<b>3</b>	<b>Results</b>	<b>10</b>
<b>4</b>	<b>Conclusions</b>	<b>17</b>
	<b>Bibliography</b>	<b>18</b>

**Abstract**

This project deals with the constrained optimisation of a winglet for a 3D original designed wing that flies at a speed of  $100\frac{m}{s}$  ( $Ma \approx 0.3$ ) in air considered incompressible. The wing studied, realised using Onshape software, has a maximum chord of 5m and a span of 10m while the winglet has a length of 1.5m and a minimum chord of 0.2m. The NACA2412 and the symmetric NACA 0012 are used, respectively, for the wing and winglet profiles. The objective is to minimise the total drag count defining the optimal winglet's Cant and Toe angles. The SimpleFOAM solver is used for the CFD simulation while Dakota environment allows performing the parametric optimisation. The polar diagram of the wing without winglet is realised to find the value of the angle of attack that maximises the  $C_L/C_D$  ratio. The parametric analysis is carried out by fixing the same angle of attack.

# 1 Physics behind

## 1.1 Lift and Drag

The lift and drag forces are the aerodynamic forces transmitted by a fluid to a defined surface of a body. The mechanism by which a fluid transmit those forces can be explained by looking at an airfoil of unit span (figure 1). It is considered an elemental surface area of the airfoil  $dS$  on which the pressure  $p$ , normal to the surface, and the shear stress  $\tau$ , tangential to  $dS$ , is applied. The elemental force vector on that surface can be expressed as [1]:

$$d\mathbf{F} = -p\mathbf{n}dS + \tau\mathbf{m}dS, \quad (1)$$

where  $\mathbf{n}$  is the versor perpendicular to the elemental surface and  $\mathbf{m}$  is the one tangential to  $dS$ , the first term expresses the pressure force on the surface while the second term expresses the shear or friction forces. To evaluate the net aerodynamic force vector acting on the full body it is required to calculate the surface integral of equation (1) over the entire airfoil surface:

$$\mathbf{F} = \iint d\mathbf{F}. \quad (2)$$

The lift (L) and drag (D) can now be evaluated as the component of  $\mathbf{F}$  in the y and x direction respectively; the lift can be express as:

$$L \approx y - \text{component} \left[ - \iint p\mathbf{n}dS \right] \quad (3)$$

the lift is mainly generated by the surface pressure distribution while the shear stress distribution makes a negligible contribution; the lift vector is always perpendicular to the flow direction. The drag instead depends on the x component of the pressure force and on the x component of the friction forces and its vector results always parallel to the flow direction. The drag can be express as:

$$D \approx x - \text{component} \left[ - \iint p\mathbf{n}dS + \iint \tau\mathbf{m}dS, \right] \quad (4)$$

where first term represent the pressure drag and the second one represent the skin-friction drag.

### 1.1.1 Lift and Drag Coefficients

The lift and drag coefficients are dimensionless parameters that express the ratio between the lift and drag forces, respectively, and the dynamics pressure. The lift and drag coefficient are functions of the shape of the body, of the Reynolds number and the fluid speed.

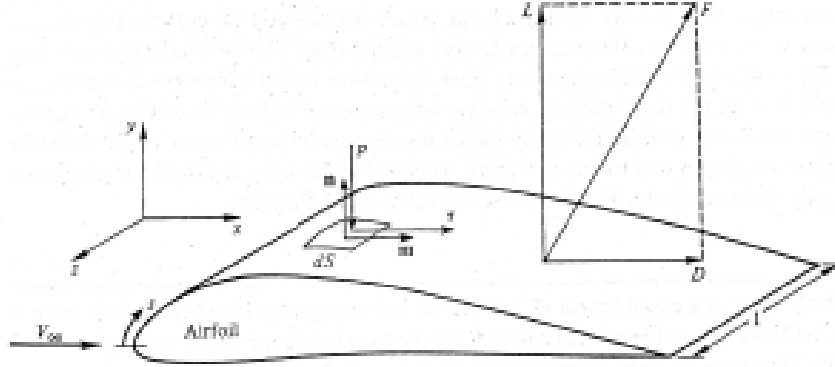


Figure 1: Lift and drag vectors presented for a wing with zero angle of attack

The lift coefficient can be expressed as:

$$C_l = \frac{L}{\frac{1}{2}\rho v_\infty^2 S}, \quad (5)$$

while the drag coefficient can be expressed as:

$$C_d = \frac{D}{\frac{1}{2}\rho v_\infty^2 A_c}. \quad (6)$$

It is important to consider that the lift coefficient is based on the relevant plane area ( $S$ ) while the drag coefficient is based on the projection of the frontal area ( $A_c$ ) on a plane perpendicular to the fluid speed.

## 1.2 Induced Drag

Since the wing has a finite dimension, the pressure gradient at the tip forces the air to flow from the pressure to the suction side. This causes the generation of counter-rotating vortex at the tips that propagates behind the aeroplane and create a down-wash force (fig.: 2). Locally the velocity changes direction and results inclined of an angle  $\alpha_i$ , the induced angle of attack can be calculated with the Prandtl correlation:

$$\alpha_i = \frac{1}{\pi e AR}, \quad (7)$$

where  $AR$  is the aspect ration and "e" is the Oswald efficiency factor that takes into account the lift distribution over the wingspan. The  $\alpha_i$  cause the effective lift ( $L_{eff}$ ) to be

inclined of  $\alpha_e = \alpha - \alpha_i$  and so the drag result increased by the new horizontal component of the  $L_{eff}$ , to the drag coefficient equation (eq.:6) is necessary to add the induced drag coefficient ( $CD_i$ ) [2]:

$$CD_i = \frac{C_l^2}{\pi e AR}. \quad (8)$$

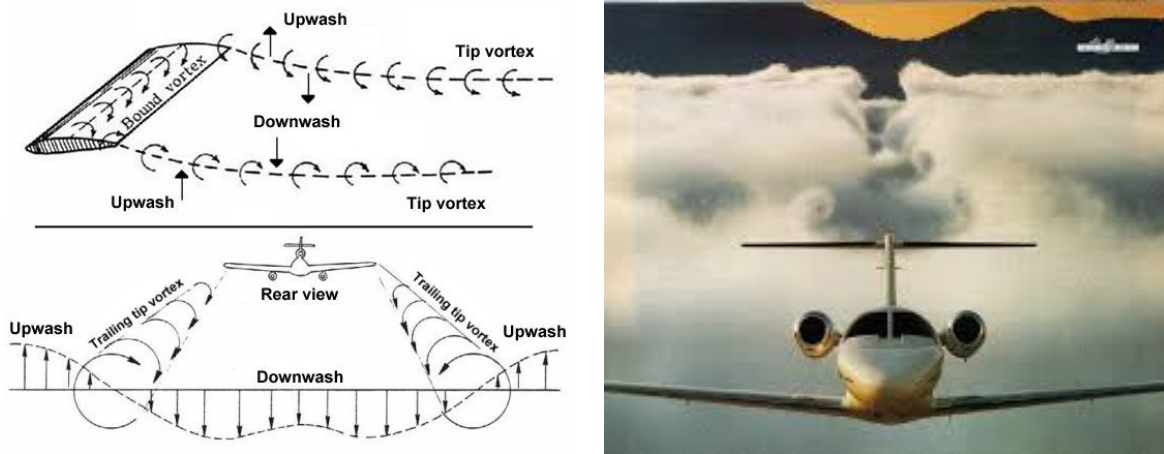


Figure 2: Sketch of the wing tip vortex and their effect (Left, font: <https://areweb.polito.it/fluidlab/teaching/thesis/bachelor/BivonaBATalk2014.pdf>). Real Picture of the wing tip vortex effect (Right, font: [www.grc.nasa.gov](http://www.grc.nasa.gov))

### 1.3 Winglets

The winglets are wing tip devices (fig.:3) that allow decreasing the pressure gradient between the pressure and the suction side of the wing tip [3]. It is possible, in this way, to reduce the wing tip vortices and the induced drag, decreasing the fuel consumption. The winglet reduces also the dimension and the intensity of the turbulent wake left behind the aeroplane. There are different winglet configuration and dimensions, each of them can optimize a precise operative condition (fig.: 3).

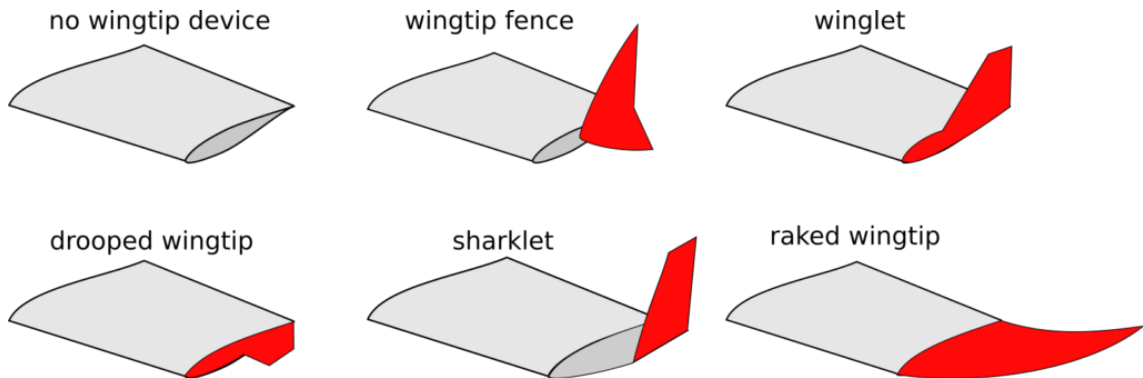


Figure 3: Possible wing tip configurations (font: <http://www.razvanapetrei.com>)

## 2 Simulation set up

### 2.1 Geometry

The geometry (4a) is realised by taking into account the standard dimensions of large plane wings without considering an existing design. It is created with Onshape environment, an online cad modelling software that allows creating and sharing projects. One of the main onshape advantages is to allow using external scripts, coded in python2 language, to modify the geometry.

As it is possible to notice from figure 4b the maximum chord of 5m is on the area that should be attached to the fuselage of the aeroplane and decrease reaching its minimum value of 0.5m at the wing tip. The leading edge has a constant inclination of  $60^\circ$  with the y-direction while the trailing edge starts perpendicular to the fuselage. This configuration allows having a smooth decreasing of the chord leaving a first area that can sustain the engine and its systems. The same NACA2412 profile is used for the entire wing while for the winglet is chosen asymmetric NACA0012. The winglet (fig.:5b) starts with a chord of 0.5m that decreases to 0.2m at the tip, the length is fixed to be 1.5m. For this project, the Cant angle can vary between  $10^\circ$  and  $90^\circ$ , the Toe angle can assume a value between  $-20^\circ$  and  $20^\circ$ , while the twist and the sweep angles have a value of zero degrees (fig.:5a).

### 2.2 OpenFOAM set up

In this section, is explained the set up used to realise the unstructured mesh for the wing with and without winglet, furthermore is explained the set up for the simpleFOAM simulation.

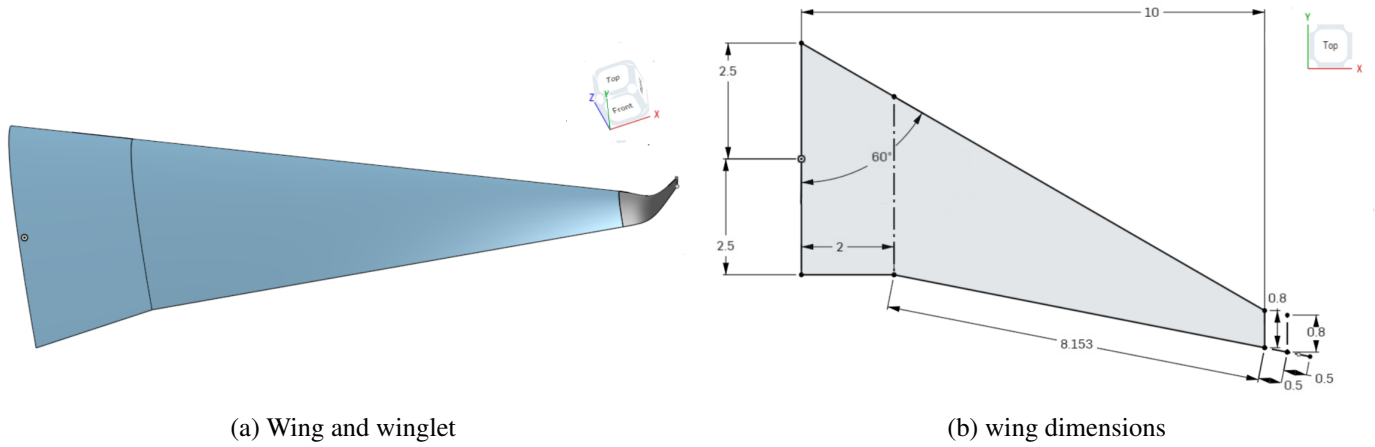


Figure 4: 3D view of the wing with the winglet (Left) and sketch of the simple wing (Right)

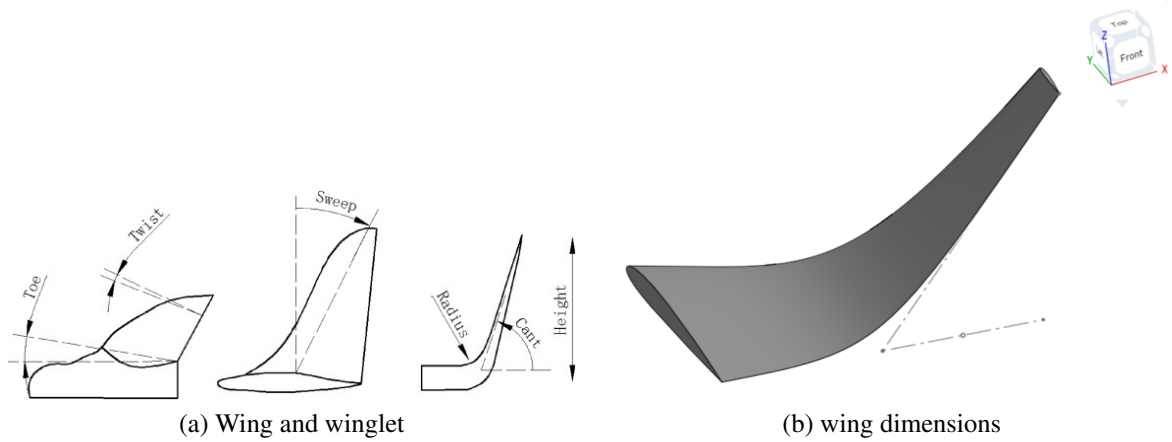


Figure 5: Sketch of the Can, Toe, twist and sweep angles (Left) and the actual winglet studied (right)

### 2.2.1 Unstructured Mesh

To study the 3D flow around the wing, a parallelepiped farfield is chosen (figure 6): 30 meters wide (x-direction), 80 meters long (y-direction) and 60 meters tall. The side of the wing that should be connected with the fuselage of the aeroplane is positioned attached to one side of the farfield (at  $x = 0$ ), the inlet plane is set 30m in front of the x-axis centre while the outlet plane is set to be 50m behind it. The wing is also placed in the centre of the z-axis.

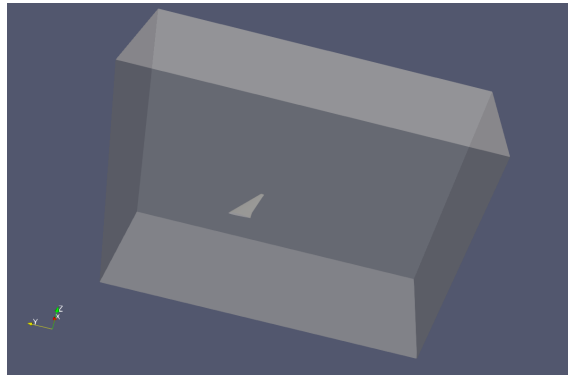


Figure 6: Full farfield with the wing placed inside

The wing and the winglet are exported from Onshape as two different *stl* files to be able to refine the mesh locally.

For the background mesh the *blockMesh* dictionary is set to generate a structured hexahedral mesh, a single block mesh is used with a subdivision to have squared cells of  $8m^3$ . All the sides of the farfield, the wing and the winglet are set on the *blockMeshDict* as patches except for the farfield side attached to the wing that has symmetry boundary condition (BC). The *surfaceFeatureExtract* feature is used to be able to approximate better the mesh close to the surface of the wing, for this purpose *includeAngle* is set to  $180^\circ$  to select all edges both for the wing and the winglet.

To complete the mesh, *snappyHexMesh* is used enabling the *castellatedMesh*, the *snapping* and the layer addition. The castellated Mesh allows to define the global, the edge, the surface based and the region-wise refinements, they are defined to have the finest mesh possible maintaining the simulation time lower than 2 hours (average of 1.5 million points). The material point that indicates where the mesh must be created, is set outside of the wing but inside of the farfield (see table 1). The layer addition is necessary to study the flow around the wing, the distance ( $Y$ ) between the wing and the first cell is precisely calculated to maintain  $Y_{plus}$  around 300:

$$Y_{plus} = \frac{U_\tau Y}{\nu}, \quad (9)$$

Where  $U_\tau$  is the friction velocity at the wall and  $\nu$  is the kinematic viscosity. In total five layers are added.

The most important parameters chosen for the *snappyHexMeshDict* can be seen in table 1 and table 2, while in figure 7 is shown the full mesh.

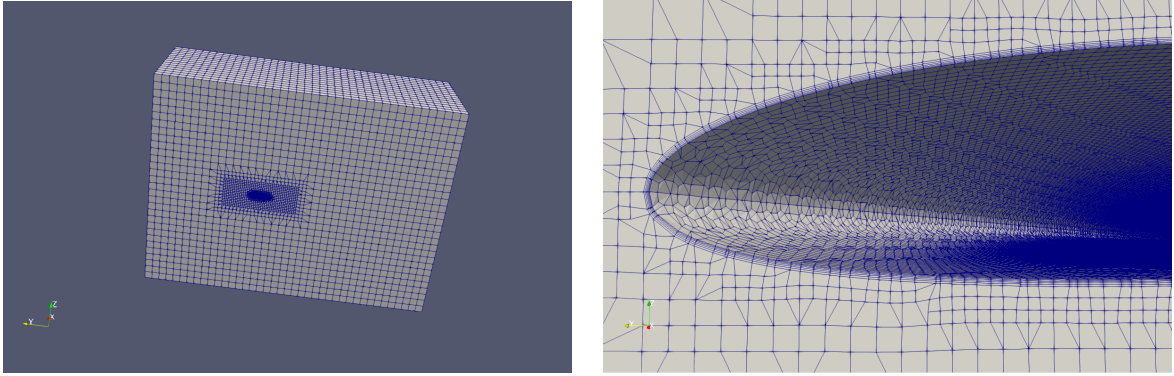


Figure 7: Full mesh of the domain (Left) and zoom on the layers around the leading edge (right)

### 2.2.2 SimpleFOAM set up

Since the case studied is a subsonic flow with  $Ma=0.3$ , the *simpleFOAM* solver is used, the same set up is defined to study the wing with and without the winglet. In table 3 are shown the boundary condition chosen for each patch for the full wing analysis, the front and back patches are not shown because they always have the same BC, respectively slip and symmetry. For the analysis of the lift and drag coefficients with respect to the angle of attack the direction of the flow is changed. With a positive  $\alpha$  the flow is entering from the inlet and bottom patches (set as inlet) and exiting from the top and outlet patches (set as the outlet). With a negative  $\alpha$  instead the bottom and top patches are set respectively as outlet and inlet. If  $\alpha = 0^\circ$  the top and bottom patches have slip conditions. The wing and the winglet surfaces have no-slip condition, and so it is possible to notice zero velocity and zero gradient pressure BC. Since the boundary layer is not fully resolved, wall functions are used both for  $k$ ,  $\nu_{t}$  and  $\omega$ .

The initial value for the turbulent kinetic energy  $k$  (TKE) was calculated as:

$$k = \frac{3}{2}(UI)^2, \quad (10)$$

where  $U$  is the free stream velocity and  $I$  is the turbulence initial estimation ( $I=1.0\%$ , low turbulence value is chosen). Once the TKE is known, it is possible to evaluate the specific

TKE:

$$\omega = \frac{\rho k \mu_t^{-1}}{\mu \mu}, \quad (11)$$

where  $\frac{\mu_t}{\mu} = 1$  is the viscosity ratio evaluated in relation to the turbulence intensity,  $\rho$  is the density and  $\mu$  is the dynamic viscosity.

The solver used for the pressure field is the GAMG one while for  $\omega$ ,  $k$  and  $U$  the *PBiCGS tab* solver was chosen. The relaxation factors are chosen all 0.7 for fields and equations.

To conclude the *controlDict* file is prepared to allow the simulation to run 500 iterations maximum, with a residual control of  $1e - 8$ , and to evaluate the forces, the forces coefficients and the  $Y_{plus}$ . For this purpose the Lift and Drag direction are defined according to the flow direction the magnitude of the free-stream velocity is set to  $100 \frac{m}{s}$  and the density is defined as  $1.225 \frac{kg}{m^3}$ . For the simple wing, the planform area is calculated with onshape (Aref= 27.426m<sup>2</sup>) as well the reference length (lRef=6.574m). Since the different configuration of the winglet change only marginally the Aref, it has been decided to average the variations and set Aref=28m<sup>2</sup> and lRef=6.7m.

### 2.3 Dakota optimization process

The optimisation process was carried on using Dakota environment connected directly with OpenFOAM and using python2 environment with Onshape. The parametric study is carried on finding the minimum value of the drag count  $\Delta C_D$  (eq.:12) with respect to variations of the Cant angle. After the minimum is found, the Cant angle is fixed, and the drag count is analysed for different Toe angles. The global minimum was checked fixing different Cant or Toe angles and evaluating if the  $\Delta C_D$  was minimum always for the same Toe or Cant angles respectively.

The process starts with Dakota that changes the geometry directly inside Onshape and exports the *stl* files. The mesh is then created, and the simpleFOAM analysis is processed. The  $C_D$  value extracted is the average of the last 50 iterations to avoid the small fluctuation that can occur at the convergence of the simulation.

$$\Delta C_D = 10^4 C_D \quad (12)$$

## 3 Results

In this section is presented the analysis carried on in order to find the angle of attack that corresponds to the minimum value of the  $\frac{C_D}{C_L}$  ratio. Then the results of the optimisation

Table 1: Castellated Mesh main parameters

<b>CastellatedMesh</b>	<b>Wing</b>			<b>Wing and Winglet</b>		
<b>refinementBox</b>	<b>x</b>	<b>y</b>	<b>z</b>	<b>x</b>	<b>y</b>	<b>z</b>
min	0	-10	-4	0	-10	-4
max	15	10	4	15	10	4
<b>refinementRegion levels</b>	(1e15 2)			(1e15 2)		
<b>location in Mesh</b>	<b>x</b>	<b>y</b>	<b>z</b>	<b>x</b>	<b>y</b>	<b>z</b>
	20	10	15	20	10	15
<b>feature level</b>	6			7 and 8		
<b>refinementSurfaces level</b>	(3 6)			(2 7) and (2 8)		
<b>resolveFeatureAngle</b>	0.01			0.001		

Table 2: Layers main control parameters

<b>Layers</b>	<b>Wing</b>	<b>Wing and Winglet</b>
<b>Number</b>	5	5
<b>minThickness</b>	0.000037	0.000037
<b>finalLayerThickness</b>	0.005	0.005
<b>expansionRatio</b>	1.2	1.2
<b>featureAngle</b>	130	130

Table 3: Constant parameter for simpleFOAM simulation on the full wing analysis with  $\alpha = 3^\circ$ 

	<b>Inlet</b>	<b>bottom</b>	<b>outlet</b>	<b>top</b>	<b>wing</b>	<b>winglet</b>
<b>K</b>	fixedValue uniform 1.5	fixedValue uniform 1.5	inletOutlet inletValue uniform 0	inletOutlet inletValue uniform 0	kqRWallFunction uniform 1.5	kqRWallFunction uniform 1.5
<b>nut</b>	calculated uniform 0	calculated uniform 0	calculated uniform 0	calculated uniform 0	nutUSpalding WallFunction uniform 0	nutUSpalding WallFunction uniform 0
<b>omega</b>	fixedValue uniform 103000	fixedValue uniform 103000	inletOutlet inletValue uniform 103000	inletOutlet inletValue uniform 103000	omega WallFunction uniform 103000	omega WallFunction uniform 103000
<b>p</b>	fixedValue uniform 0	fixedValue uniform 0	zeroGradient	zeroGradient	zeroGradient	zeroGradient
<b>u</b> ( $\alpha = 3^\circ$ )	fixedValue uniform (0 -99.8630 5.2336)	fixedValue uniform (0 -99.8630 5.2336)	zeroGradient	zeroGradient	fixedValue uniform ( 0 0 0)	fixedValue uniform ( 0 0 0)

process are presented, and the polar is also defined for the full wing.

In figure 8 is possible to notice the different values for the lift and drag coefficients for the simple wing at different angles of attack ( $-8^\circ < \alpha < 30^\circ$ ). Since the profile of the wing is a NACA2412, the zero lift angle of attack results for  $\alpha = -2.1^\circ$  and, as expected, the maximum  $C_L$  occurs for  $\alpha = 15^\circ$ ; the analysis continues until  $\alpha = 30^\circ$ . At  $\alpha = 17^\circ$  the flow separates at the tip of the wing and only after  $\alpha = 25^\circ$  we can notice the full separation of the boundary layer around the entire wing. After the definition of the drag and lift coefficients in relation with the angle of attack (fig.: 8b), it was possible to evaluate both the polar (fig.: 8c) and the  $C_L/C_D$  ratio (fig.: 8d). With  $\alpha = 3^\circ$  the  $C_L/C_D$  ratio reaches its highest value of 25.28, at this angle of attack  $C_D = 0.01627$  and  $C_L = 0.41181$ , so the angle of attack for the winglet optimization is fixed at  $3^\circ$  to simulate a cruise flight.

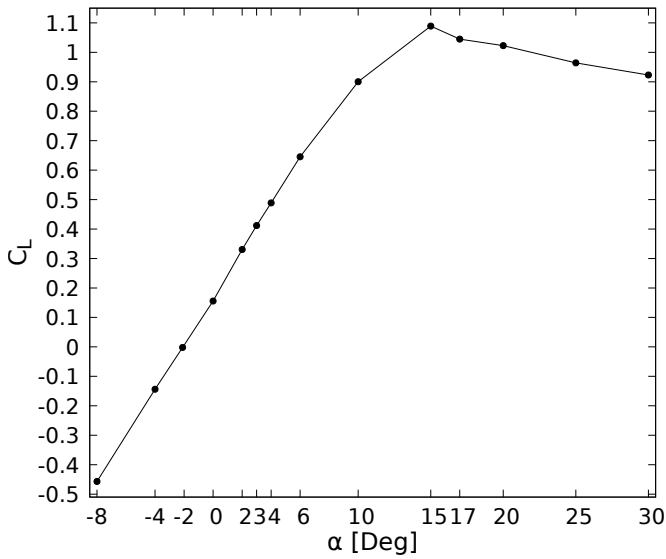
The drag count with  $\alpha = 3^\circ$  is 162.7, and it is possible to see, from figure 9 how the winglet can reduce it drastically. The first analysis was carried setting the Toe angle to zero degrees (fig.: 9a), and it is possible to see that the minimum value of the  $\Delta C_D$  was found for a Cant angle of  $25^\circ$ . Fixing the Cant angle to  $25^\circ$ , the effect of the variation of the Toe angle has been evaluated and in figure 9c it is possible to notice that the drag count curve resembles a parabola and the minimum can be found for a Toe angle of  $4^\circ$  [3].

To define if the minimum found for Cant= 25° and Toe=4° is a global one, different simulations were carried by fixing the Toe or the Cant angle; in figure 9b is shown the variation of the drag count with a Toe angle of 4°. The minimum is always found for a Cant angle of 25° and a Toe angle of about 4°. In figure 9d it is possible to notice how the minimum drag count is found for a Toe angle of 6° and a Cant angle of 50°. Decreasing the Cant angle the minimum shift to 4°. The comparison between the different simulations can be seen in figure 10. The global minimum has a drag count value of  $\Delta C_D = 136.69$  and is found for a Toe angle of 4° and a Cant angle of 25°.

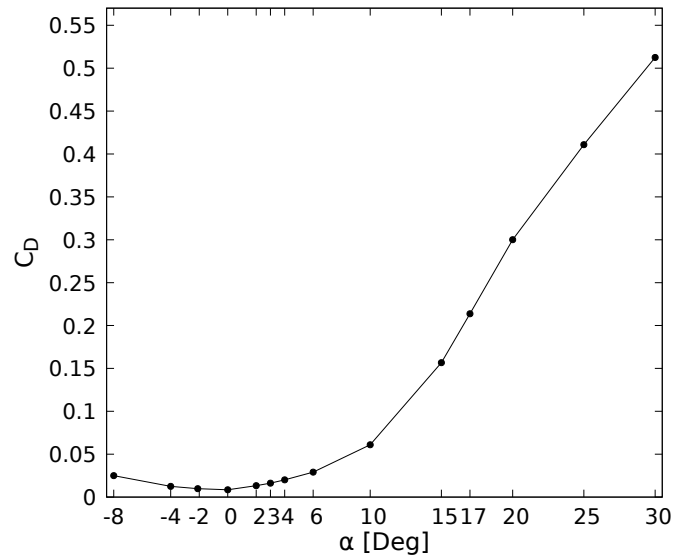
After the simulation process was concluded, the polar was defined (fig.: 11). It is interesting to notice how the winglet results optimal for all the positive angle of attack and the crossing point is found only for negative  $\alpha$ ; this last result shows that the winglet is optimal for all the operative condition and it is perfect for cruise flight. Looking at the lift coefficient, it is possible to notice that it slightly increases with respect to the simple wing and becomes higher increasing  $\alpha$ , for the cruise flight ( $\alpha = 3^\circ$ )  $C_L = 0.4156$  and the ratio  $C_L/C_D$  results equal to 30.4. To conclude the vorticity magnitude can be evaluated for both the wing with and without the winglet in planes at the same distance from the trailing edge of the wing. In figure 12 it is possible to notice that in the case with the winglet the vortex seems wider but has a lower magnitude and so it disappears rapidly, while in the wing without winglet the vortex remains almost constant with a higher intensity.

$\alpha = 3^\circ$	<b>Simple Wing</b>	<b>Wing &amp; Winglet</b>
$C_L$	0.412	0.416
$\Delta C_D$	162.7	136.7
$C_L/C_D$	25.28	30.4

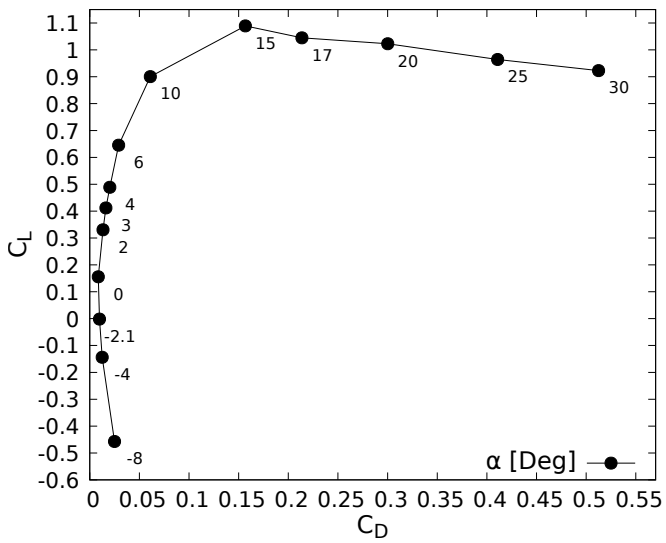
Table 4: Comparison of the lift coefficient, the drag count and the lift over drag coefficient ration for the wing with and without winglet at  $\alpha = 3^\circ$ .



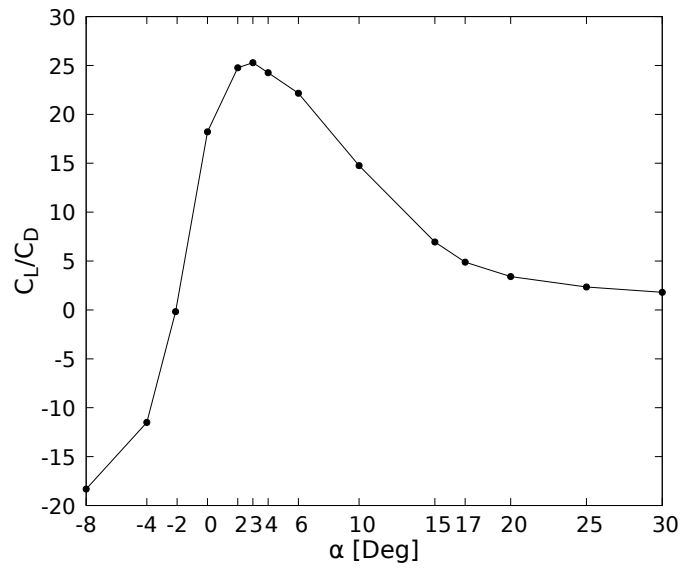
(a) Lift coefficient against  $\alpha$



(b) Drag coefficient against  $\alpha$

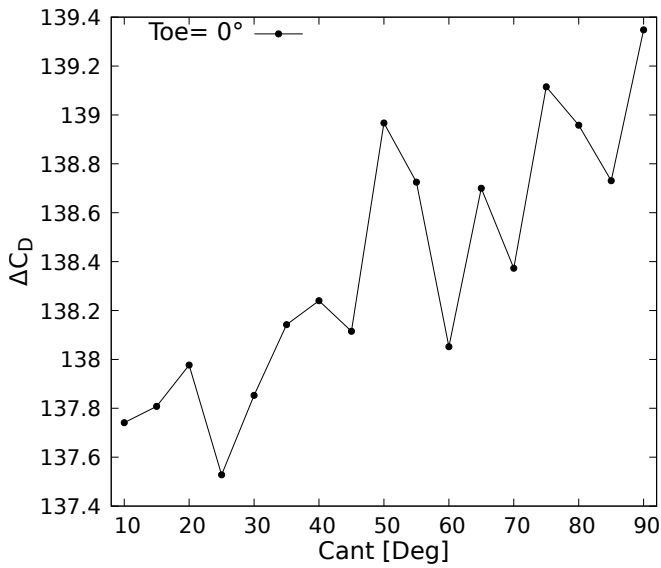


(c) Wing polar  $\alpha$

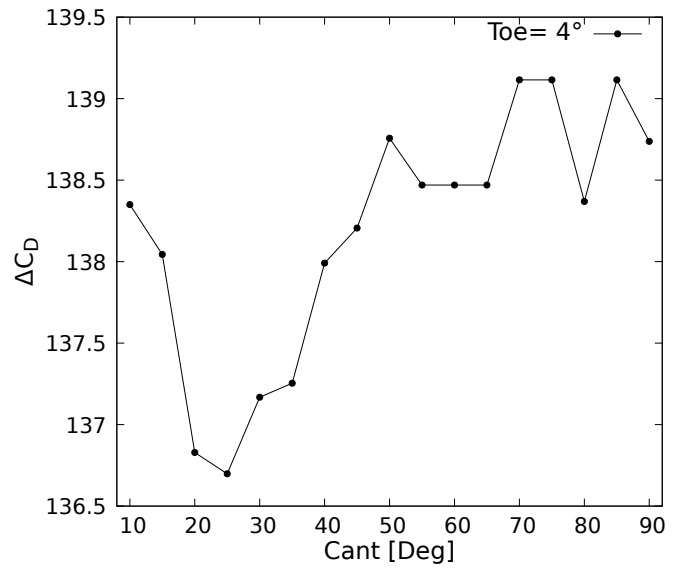


(d) Lift to drag coefficients ratio against  $\alpha$

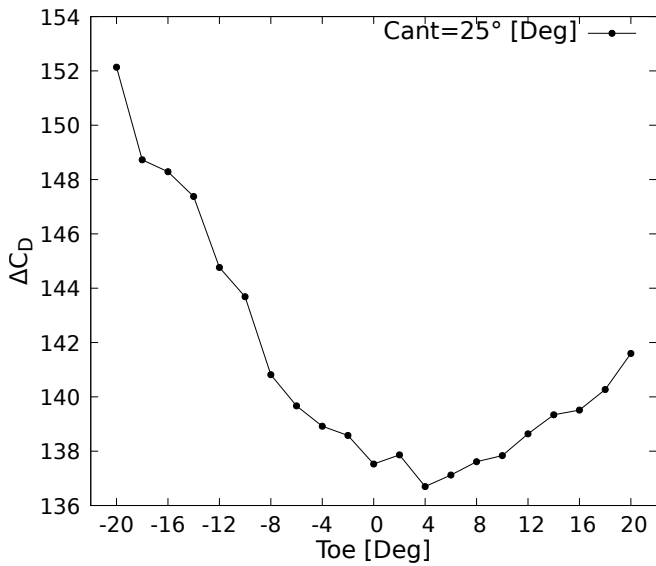
Figure 8: Analysis of the lift and drag coefficients with different angle of attack.



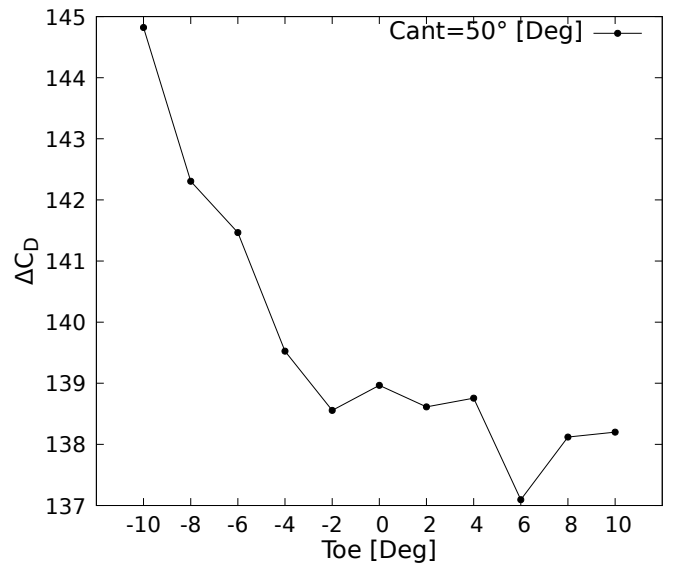
(a)  $\Delta C_D$  with different Cant angle and Toe = 0°



(b)  $\Delta C_D$  with different Cant angle and Toe = 4°



(c)  $\Delta C_D$  with different Toe angle and Cant = 25°



(d)  $\Delta C_D$  with different Cant angle and Cant = 50°

Figure 9: Drag Count variation with different Cant and Toe angles.

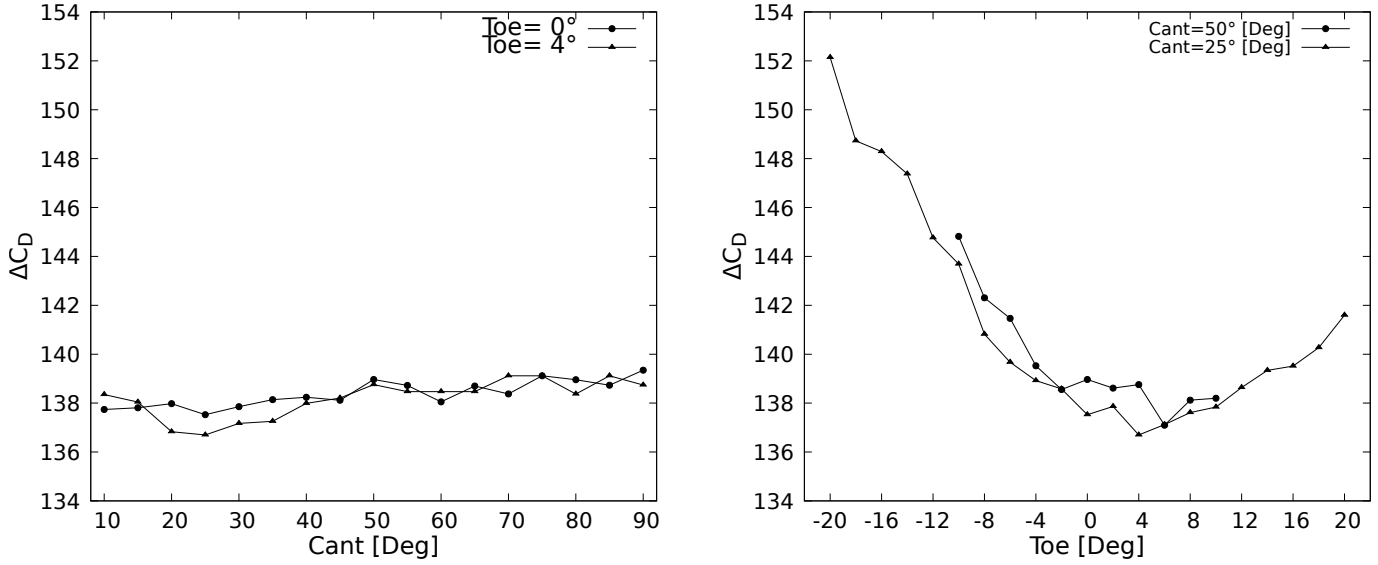


Figure 10: Comparison of the different analysis done, with Toe angle constant (Left) and with Cant angle constant (Right).

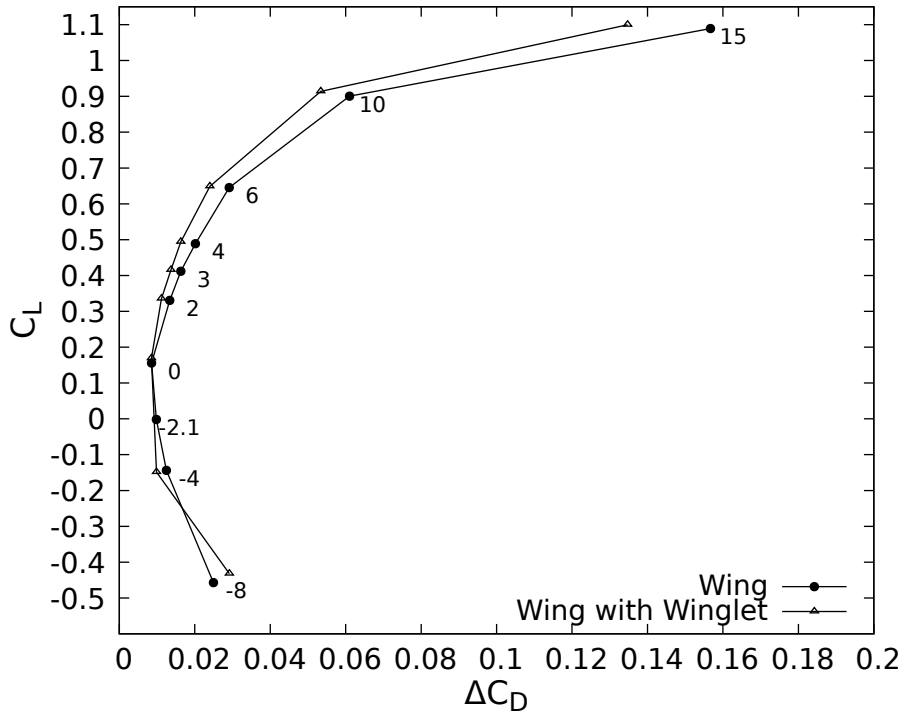


Figure 11: Comparison between the polar of the wing without and with winglet.

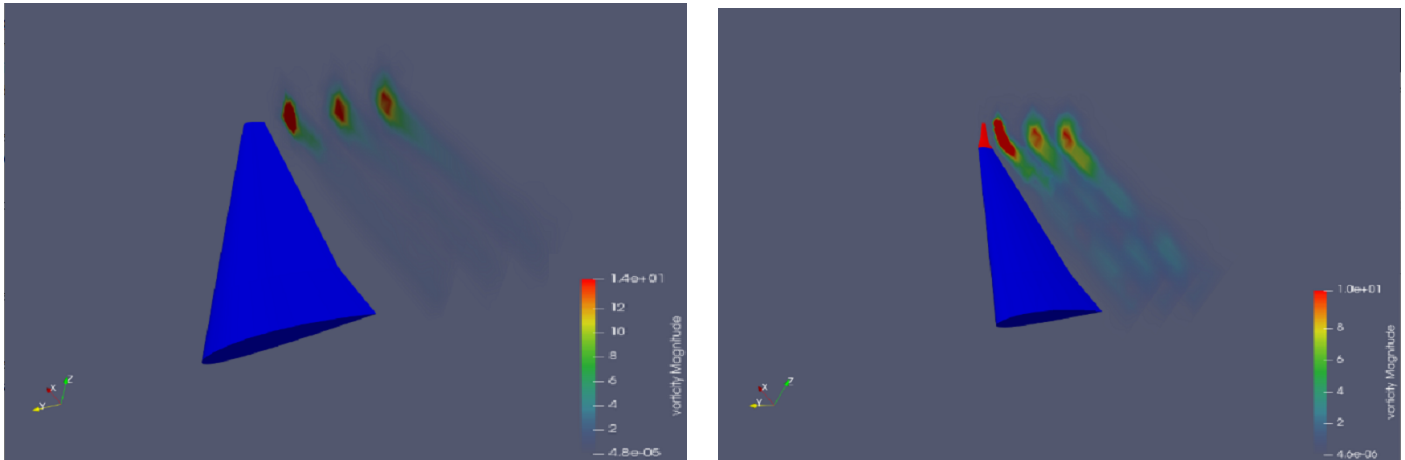


Figure 12: Comparison between the vorticity behind the wing with and without winglet.

## 4 Conclusions

In conclusion, it is possible to state that for the wing studied (fig.:4) during a flight at  $Ma=0.3$  and with an angle of attack of  $3^\circ$ , the optimal configuration of the winglet has a Cant angle of  $25^\circ$  and a Toe angle of  $4^\circ$ . This solution allows to reduce the drag count to 136.69 and results optimal for the cruise phase since the crossing point of the polars is below zero. A great drag reduction is possible with the winglet that makes the ratio  $C_L/C_D$  to increase by 5 points. The vorticity magnitude is also reduced thanks to the winglet used.

## References

- [1] J. D. Anderson. *Modern Compressible Flow: With Historical Perspective*. McGraw-Hill Education, Boston, 3 edition, 2002. ISBN 978-0-07-242443-0.
- [2] John D. Anderson Jr. *Introduction to Flight*. McGraw-Hill Education, 7 edition, June 2011. ISBN 978-81-8473-392-1.
- [3] M. D. Maughmer, T. S. Swan, and S. M. Willits. Design and Testing of a Winglet Airfoil for Low-Speed Aircraft. *Journal of Aircraft*, 39(4):654–661, 2002. ISSN 0021-8669. doi: 10.2514/2.2978. URL <https://doi.org/10.2514/2.2978>.